In silico Prediction on the PI3K/AKT/mTOR Pathway of the Antiproliferative Effect of *O. joconostle* in Breast Cancer Models

Alejandra Ortiz-González[1], Pedro Pablo González-Pérez[2] (iD),
Maura Cárdenas-García[1] (iD)
and María Guadalupe Hernández-Linares[3] (iD)

[1]Laboratorio de Fisiología Celular, Facultad de Medicina, Benemérita Universidad Autónoma de Puebla, Puebla, PUE, México. [2]Departamento de Matemáticas Aplicadas y Sistemas, Universidad Autónoma Metropolitana, Unidad Cuajimalpa, México. [3]Laboratorio de Investigación del Jardín Botánico, Centro de Química, Instituto de Ciencias, Benemérita Universidad Autónoma de Puebla, Puebla, PUE, México.

ABSTRACT: The search for new cancer treatments from traditional medicine involves developing studies to understand at the molecular level different cell signaling pathways involved in cancer development. In this work, we present a model of the PI3K/Akt/mTOR pathway, which plays a key role in cell cycle regulation and is related to cell survival, proliferation, and growth in cancer, as well as resistance to antitumor therapies, so finding drugs that act on this pathway is ideal to propose a new adjuvant treatment. The aim of this work was to model, simulate and predict *in silico* using the Big Data-Cellulat platform the possible targets in the PI3K/Akt/mTOR pathway on which the *Opuntia joconostle* extract acts, as well as to indicate the concentration range to be used to find the mean lethal dose in *in vitro* experiments on breast cancer cells. The *in silico* results show that, in a cancer cell, the activation of JAK and STAT, as well as PI3K and Akt is related to the effect of cell proliferation, angiogenesis, and inhibition of apoptosis, and that the extract of *O. joconostle* has an antiproliferative effect on breast cancer cells by inhibiting cell proliferation, regulating the cell cycle and inhibiting apoptosis through this signaling pathway. *In vitro* it was demonstrated that the extract shows an antiproliferative effect, causing the arrest of cells in the G2/M phase of the cell cycle. Therefore, it is concluded that the use of *in silico* tools is a valuable method to perform virtual experiments and discover new treatments. The use of this type of model supports *in vitro* experimentation, reducing the costs and number of experiments in the real laboratory.

KEYWORDS: Modeling and simulation, *in silico* prediction, *in vitro* evaluation, cell signaling pathways, breast cancer

Introduction

Breast cancer presents a health problem worldwide, for the year 2020 it has been determined to be the most commonly diagnosed cancer worldwide, being the disease that ranks first in terms of incidence. It was detected in 1 in 8 patients with tumors, with 2.3 million new cases and is considered the fifth leading cause of death from cancer in the world with 685 000 deaths per year, representing 1 in 6 cancer deaths.[1]

Breast cancer is the leading cause of death from malignant neoplasms in Mexican women, constituting between 20% to 25.7% of all cancer cases detected in women.[2] In 2020 an increase in new cases was reported, as well as an increase in the number of deaths from this type of cancer; figures are related to the lifestyle and bad habits acquired by the Mexican population.[1]

The search for new novel adjuvant treatments, accessible to a larger part of the population, with mild side effects implies the development of studies that allow the evaluation of pharmaceutical effects, by understanding the molecular mechanisms underlying cancer. For this purpose, different cell signaling pathways have been described and analyzed, which are key points in the understanding of cancer, since signal transduction is involved in the control of the cell cycle, as well as proliferation, survival, apoptosis and, therefore, knowing all these regulatory systems allows us to propose treatments against cancer.[3,4]

Among the main signaling pathways related to breast cancer are the PI3K/Akt/mTOR pathway, the canonical Wnt pathway and Notch pathway. Among these pathways, the PI3K/Akt/mTOR is the one that is most frequently modified in breast cancer (more than 60% of tumors)[5,6] mainly by mutation of the PIK3CA gene.[7]

The PI3K/Akt/mTOR pathway plays a key role in cell cycle regulation and is directly related to cell survival, proliferation, growth and motility in cancer, as well as cell resistance to antitumor therapies.[8] The pathway is activated by binding of a

Table 1. Relationship of the models of 10 main signaling pathways, using Gillespie's stochastic simulation algorithm.

PATHWAY	TOOL	SOURCE
RTK/RAS/JAK/STAT	Parallel Select algorithm SSA stochastic expectation-maximization algorithm SSA	Bouhaddou et al,[32] Ganesan et al,[33] Sehl et al,[34] Sabbe et al,[35] Liu et al[36]
Nrf2	LNT	Calabrese et al[37]
TGF	Differential equations	Khatibi et al[38]
PI3K/AKT/mTOR	SSA Boolean network model/stochastic	Bouhaddou et al,[32] Zielinski et al[39]
Wnt	SSA Differential equations Differential equations Multiscale	Haack et al,[40] Kogan et al,[41] Vargas et al,[42] Agur et al[43]
Myc	Dynamic network	Gérard et al[44]
Notch	SSA	Kay et al[45]
Hippo	Boolean model Differential equations	Gou et al[46]
p53	Boolean model ruled-based model	Gupta et al,[47] Gong et al[48]
Cell cycle	SSA Markov chain	Elizalde et al[49]

Abbreviations: SSA (stochastic simulation algorithm) LNT (linear no-threshold).

cytosine to the thyrokinin receptor kinase, leading to the activation of PI3K, which, once activated, converts phosphatidylinositol 3,4-bisphosphate to 3,4,5-triphosphate, which activates PDK1 kinase leading to Akt activation.[9] Once Akt is in its active state, phosphorylation of Akt and mTOR complex 1 takes place, causing a series of responses that through different pathways lead to cell proliferation and inhibition of apoptosis.[10,11] On the other hand, PI3K can also be activated by cytosine receptor which, once bound to its ligand, activates Janu kinases, JAK that function as tyrosine kinases activating other pathways that also lead to the activation of PI3K and the activation of the transcription factor STAT that forms a homodimer, which is translocated to the nucleus and binds to genes that encode for proteins involved in cell proliferation.[12,13]

Gillespie's stochastic simulation algorithm (SSA)[14,15] has been widely used to simulate cell signaling pathways, since these pathways occur in a dynamic system and are chemical reactions. Over time different tools have been developed to simulate cell signaling having SSA as a basis, such as Dizzy,[16] Toolbox,[17] Copasi,[18,19] STEPS,[20] ERODE,[21] CoLoMoTo,[22] MONALISA that implements SSA in a Petri net environment.[23] In principle, this algorithm assumes that all reactions occur instantaneously in a homogeneous medium, although the reactions are affected by different factors such as cell size, organelles (cell compartments), the distribution of molecules in each of the cell compartments, the affinity between reactants, among others, so different research groups have modified this SSA, for example introducing the state-dependent weighted stochastic simulation algorithm (swSSA) and the doubly weighted SSA (dwSSA), the weighted SSA (wSSA).[24] The Extra Reaction algorithm for Networks in Dynamic Environments has been added to the SSA which allows exact stochastic simulation of any downward reacting network, according to the different choices of dynamic inputs that are simulated in advance.[25] Other groups consider that the computational cost is very high employing SSA, given the complexity of the signaling pathways, so they have developed algorithms that provide speed in processing, without losing detail such as BISSSA (block search stochastic simulation algorithm).[26] Cell signaling pathways have also been represented as production rule systems with molecular interactions governed by SSA and Markov chain behavior.[27,28]

Within the cell, in the cell cytoplasm, proteins involved in signaling pathways are produced and diffuse within a limited space. Some proteins they must interact with are membrane-anchored,[29] so models have been proposed in the third dimension[52] or in different physiological conditions.[15] Other models consider specific cellular events, identifying signaling pathways that take place during these events, such as cell migration.[30]

The regulatory mechanisms of cancer cells remain a mystery, despite all the research carried out so far. This is because they are constantly changing, so predicting their behavior is not easy, the alterations and combinations are very broad, even in the same type of cancer and come from the same tissue. This results in a complex interaction between signaling pathways that under normal conditions would not be observed; these interactions provide information on the regulation that occurs stochastically.

The main signaling pathways that play a relevant role in the regulation of cell communication in cancer are 10.[31] Table 1 shows a list of the models proposed in the literature for these signaling pathways using Gillespie's stochastic simulation algorithm. The goal of modeling these pathways is to predict

their behavior in order to prevent the continued development of cancer cells and to provide targeted and timely therapy by identifying interacting elements.

In recent years, modeling and simulation of cell signaling systems have had to satisfy a range of new requirements that characterize this type of biological system, such as multi-compartmentalization, localization, topology and synchronization. This has led to the development of new models and computational tools. Examples of simulators supporting some of these features are Bio-PEPA,[50] MCell,[51] COPASI,[18] Virtual Cell,[52] CompuCell 3D,[53] and Big-Data Cellulat,.[54-57]

Based on Gillespie's algorithm,[14] as an engine for the selection and execution of chemical reactions, and on the spaces of tuples,[58,59] for the representation of chemical reactions and reactants, the Big-Data Cellulat computational simulation platform (http://bioinformatics.cua.uam.mx/site/) constitutes a bioinformatics virtual laboratory for the development of *in silico* experimentation in cell signaling systems, characterized by the robustness, accuracy and flexibility provided by both techniques. The *in silico* experimentation environment supported by the Big-Data Cellulat platform includes tools for the simulation, exploration, analysis, and prediction of this type of biological system; in addition to the production, pre-processing, and recording of large volumes of data generated by the simulation, for subsequent analysis based on data mining and deep learning techniques.

In this work, we discuss and illustrate the important role played by computational simulation and the corresponding *in silico* experimentation in breast cancer research. In particular, we refer to the great support provided by the Big Data-Cellulat platform in (1) the simulation of the PI3K/Akt/mTOR signaling pathway, characterized for its anti-apoptotic role in breast cancer, (2) the prediction of the antiproliferative effect of *Opuntia joconostle* (xoconostle) in breast cancer cell lines, based on the simulation of PI3K/Akt/mTOR, and (3) the *in vitro* evaluation of the mean lethal dose predicted by *in silico* experiments. In this study, a hypothesis based on the phytochemical composition of Opuntia joconostle and the possible targets of the PI3K/Akt/mTOR signaling pathway was proposed for *in silico* prediction and subsequent *in vitro* evaluation. The mean lethal dose predicted by the *in silico* model allowed us to verify the lethal concentration 50 (LC_{50}) *in vitro*, as well as to demonstrate the veracity of the hypothesis.

Material and Methods

Big-Data Cellulat: The computational simulation tool

The Big-Data Cellulat computational tool is based on the concept of tuple space for the representation and interaction of chemical reactions and reactants, and on a version of the Gillespie algorithm for the selection and execution of chemical reactions (http://bioinformatics.cua.uam.mx/site/). The joint use of these 2 approaches allows Big-Data Cellulat to exhibit a number of key features required in the simulation of cell signaling systems and subsequent *in silico* experimentation. While, on the one hand, the tuple space-based representation provides the simulation with features such as multi-compartmentalization, localization, and topology, on the other hand, the Gillespie algorithm-based selection and execution of chemical reactions (as formulated later in expressions (1) to (4)) provides the simulation with synchronization, timing, and selection based on both the speed/affinity of the chemical reaction and the availability of reactants.

Representation of the chemical reactions and reactants. As previously mentioned, the representation and interaction of chemical reactions and reactants in Big-Data Cellulat are based on the model of tuple spaces.[58-60] In a space of tuples, the interaction and synchronization between agents—functions, procedures, objects, programs, etc.—takes place through reading, modifying, writing and owning/destructing tuples in the shared tuple space. A characteristic of tuple spaces, as shared memory, is given by the decoupling that characterizes the communication and interaction between agents. That is, the agents communicate through the shared tuple space and not directly with each other. A tuple is an ordered collection of pieces of information or knowledge, which represents some relevant aspect for the coordination between agents. Based on these considerations, the structure of the model of cell signaling based on tuple spaces is illustrated in Figure 1; in a complementary way, Table 2 describes the translation of the structures and elements involved in cell signaling to tuple space abstractions.

Selection and execution of the chemical reactions. As previously mentioned, the selection and execution of chemical reactions is coordinated by an action selection mechanism based on Gillespie's algorithm,[14] where a chemical system is viewed as a distinct well-mixed solution. Every molecule is explicitly represented, and every reaction in which they can participate is explicitly simulated using Gillespie's stochastic simulation technique (SSA). The simulation then chooses the next reaction to occur based on a random number and its propensity function, which is determined based on the reaction rate and the number of reactants, once the system has been started, that is, molecules, reactions, and reaction rates have been defined. The time interval for updating the simulation time is likewise calculated step by step using a random integer and the total of all reactions' propensity functions. The simulation is made up of iterations of these phases. The main steps taken by the action selection mechanism for signal transduction are listed below in detail.

1. Determine the rate for each suitable chemical reaction using the expression (1):

$$Rate_j = RateConstant * \prod_{i=1}^{k} \binom{Mol_i}{reqMol_i} \tag{1}$$
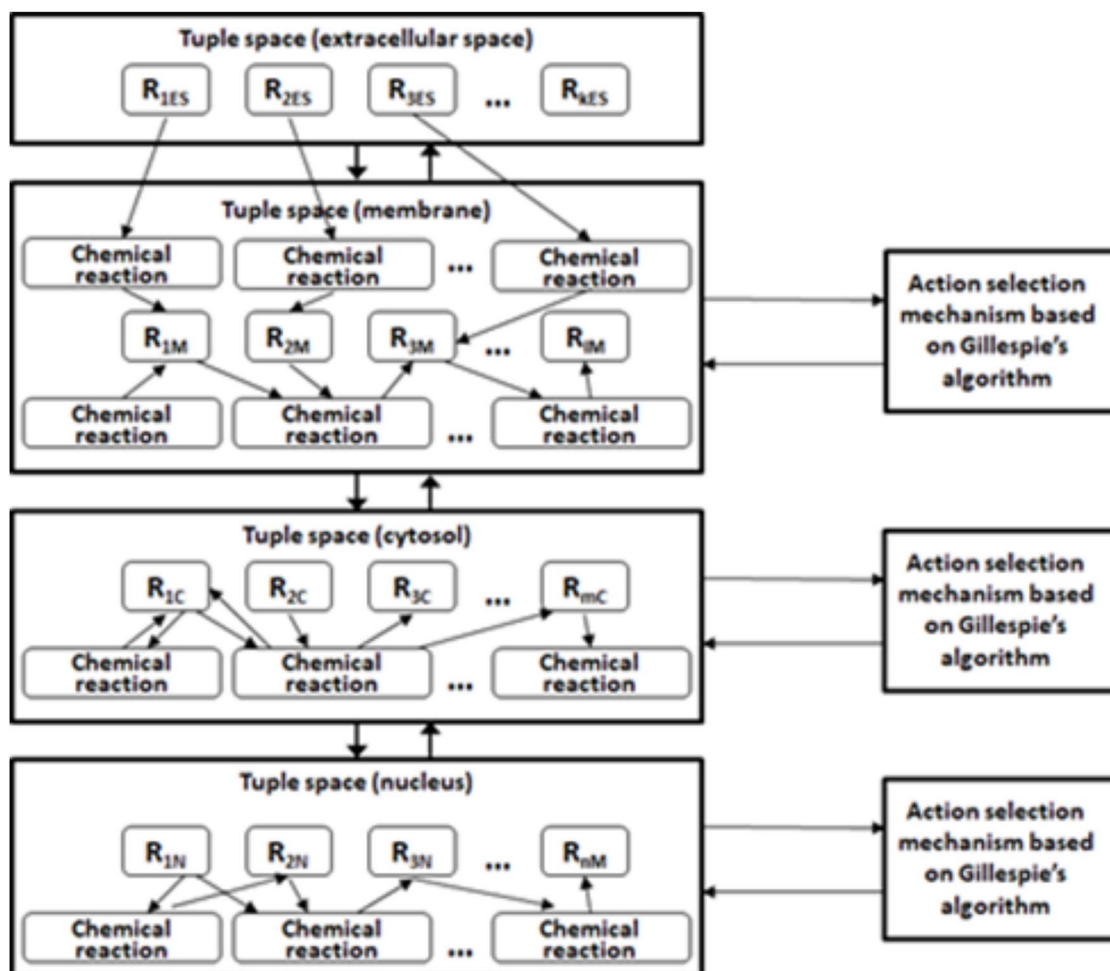
Figure 1. Use of tuple space for the representation of cellular compartments, reactants and chemical reactions involved in cell signaling. Note that the selection and execution of chemical reactions is coordinated by an action selection mechanism based on Gillespie's algorithm.

Table 2. Representation of the structures and components involved in cell signaling as abstractions of the tuple space model.

STRUCTURES AND COMPONENTS INVOLVED IN CELL SIGNALING	TUPLE SPACE MODEL ABSTRACTIONS
Intracellular compartments (ie, extracellular space, cell membrane, cytosol, nucleus, mitochondria, etc.), cells and tissues.	Tuple space
Interactions of the activation/inhibition type or compound formation between signaling elements, such as ligand-receptor, receptor- protein, protein-protein, protein-transcription factor, etc.	Sets of chemical reactions as formulated below in expression (4) to (10)
Signaling elements and their molar concentration values (ie, ligands, second messengers, proteins, substrates, etc.)	Tuples

where:

- *RateConstant* is the rate constant of the reaction
- Mol_i is the number of available molecules of reactant i, $1 \leqslant i \leqslant k$
- $reqMol_i$ is the number of required molecules of reactant i, $1 \leqslant i \leqslant k$.

The rate at which the reaction will be chosen is equal to the product of the binomial coefficients of the available moles of each reactant involved in the reaction and the number of moles required by the reaction (*RateConstant*). If any of the reactants are not present, the rate of the reaction will be 0.

2. Add the rates of all qualifying reactions together; the result is RTot.
3. Sort all qualifying reactions in descending order by rate.
4. Choice a number ψ between 0 and 1 at random.
5. The i-th reaction is selected from a sorted list of eligible reactions if:

$$\psi \leq \frac{\sum_{i=1}^{n} Rate_i}{RTot} \qquad (2)$$
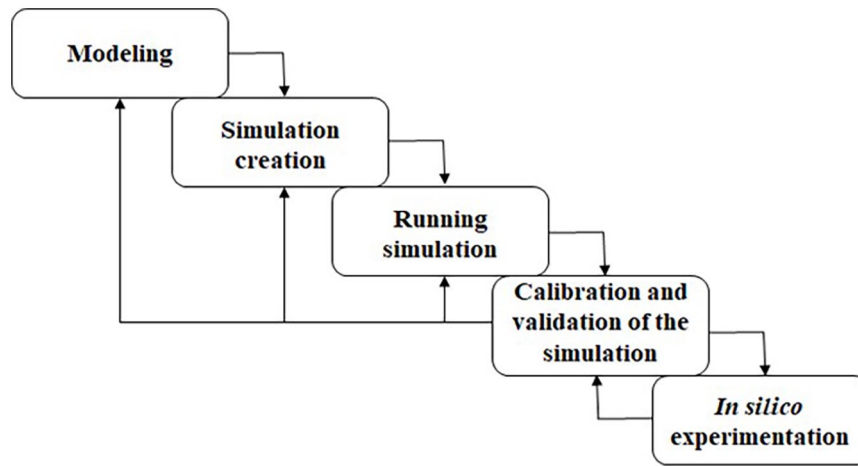
Figure 2. Phases of the modeling and simulation methodological approach.

where:

- ψ is a random number, $0 \leqslant \psi \leqslant 1$
- *RTot* is the sum of the rates (*Rate$_i$*) of all reactions

It's worth noting that the summation value for the last reaction in the sorted list is 1, implying that if there are qualifying reactions, one of them will always be executed.

6. Choice a number between 0 and 1 at random. Stop the reactions for the amount of time specified by expression (3)

$$Stop_{time} = \frac{-ln(\tau)}{RTot} \qquad (3)$$

where: τ is a random number, $0 \leqslant \tau \leqslant 1$.

The functionality of Big-Data Cellulat. Big-Data Cellulat, as a virtual bioinformatics laboratory, provides the user (biologist, biochemist, researcher in the biomedical area, life sciences, etc.) with the necessary support for:

- Simulation and comprehensive visualization of the complicated structure and dynamics of cell signaling pathways and networks.
- Visualization (through graphs, concentration/time curves and tables) of the state of activity of the global signaling network, of the interactions that occur between the different signaling elements and the variations of their states (concentration, activity, etc.) over time.
- Prediction of the cellular level effects (eg, proliferation, cell death, apoptosis, etc.) of changes and perturbations in the system in real time, which include variation in the molar concentration of signaling elements, mutations to proteins, inclusion of other signaling elements in the global network, total elimination of signaling elements (virtual knock-out).

- Design of *in silico* experiments involving the inclusion and interaction of new chemical reactions and reactants.
- The production, pre-processing and recording of large volumes of data (big data/data farming) for subsequent use in data mining, deep learning, etc.

Modeling and simulation methodology

The approach followed for the modeling and simulation of the PI3K/Akt/mTOR signaling pathway and subsequent *in silico* experimentation, based on the Big-Data Cellulat platform, comprises the phases illustrated in Figure 2. The activities involved in each of these phases are described below.

Modeling phase

1) Creation of the conceptual model. Modeling of the network that represents the cell signaling system, identifying all the signaling elements (nodes), as well as the interactions (arcs) and types of interactions (activation, inhibition, complex formation, etc.). The result of this first modeling step is a graph composed of nodes (signaling elements) and arcs (interactions between signaling elements) that represents the structure and behavior of the signaling network under study.

2) Definition of cellular structures (commonly, cellular compartments), chemical reactions, kinetic parameters, reactants, and initial micromolar concentrations, that describe and complement the conceptual model initiated in step 1).

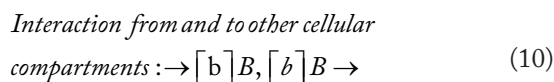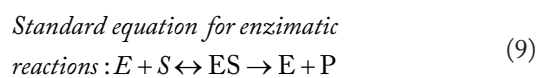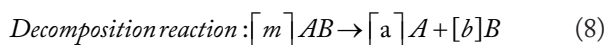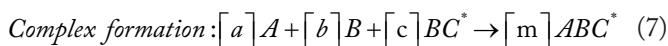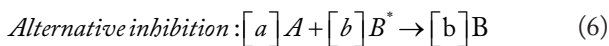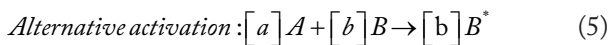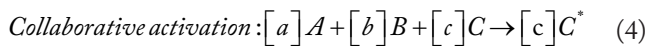Cellular compartments are the intracellular structures where reactions take place. Examples of these are cell membrane, juxtamembrane region, cytosol, nucleus, and mitochondria.

For the formulation of the chemical reactions consider expressions (4) to (10).

Table 3. Definition of reactions, reactants, and kinetic parameters for the PI3K/Akt/mTOR signaling pathway.

REACTION	REACTANTS	INITIAL CONC. (μMOL)	K_M (μMO)	V_{MAX} (μMOL/μL/S)	V_0
Cyt + RK → CytRK	Cyt RK	0.1 0.25	34.2	7.6	2.22×10^{-5}.[61]
CytRK + JAK → CytRKJAK*	JAK Cyt RK	0.012 0.0001 0.25	34.2	7.6	2.22×10^{-5}.[61]
CytRKJAK* + STAT → CytRKJAK* + STAT*	STAT Cyt RK	0.4 0.0001 0.25	74.1	49	6.61×10^{-5}.[62]
STAT* → PROLIFERATION	STAT*	0.4	74.1	49	0.263087.[62]
RAS* + PI3K → PI3K*	PI3K RAS	0.9 0.8	53.4	49	0.091588.[63]
PI3K* + PIP3 + PDK1 → PDK1*	PDK1 PIP3 PI3K	1 0.27 0.1	36	22.3	0.602702.[64]
Akt* + p21* → p21	p21 Akt	0.27 0.2	7.8	8.4	0.281040.[3]
p21 → ACTIVATION OF CELL CYCLE	p21	0.27	7.8	8.4	0.281040.[65]

Note that the reactions that model the effect of xoconostle extract are not yet considered.

$$Collaborative\ activation : [a]A + [b]B + [c]C \rightarrow [c]C^* \quad (4)$$

$$Alternative\ activation : [a]A + [b]B \rightarrow [b]B^* \quad (5)$$

$$Alternative\ inhibition : [a]A + [b]B^* \rightarrow [b]B \quad (6)$$

$$Complex\ formation : [a]A + [b]B + [c]BC^* \rightarrow [m]ABC^* \quad (7)$$

$$Decomposition\ reaction : [m]AB \rightarrow [a]A + [b]B \quad (8)$$

$$Standard\ equation\ for\ enzimatic$$
$$reactions : E + S \leftrightarrow ES \rightarrow E + P \quad (9)$$

$$Interaction\ from\ and\ to\ other\ cellular$$
$$compartments : \rightarrow [b]B, [b]B \rightarrow \quad (10)$$

where:

- [x] is the required number of molecules of reactant X.
- X is the reactant identification.
- The superscript * denotes activation of the signaling element.

Each of the reactions that takes place in the PI3K/Akt/mTOR signaling pathway was formulated for modeling and simulation taking into account the following parameters:

- K_M: the substrate concentration for which the reaction speed is half that of the maximum speed. This parameter also gives us an idea of the affinity that the enzyme has for its substrate.
- V_0: the initial speed which depends on the K_M.
- V_{MAX}: indicates the speed that we would obtain when all the enzyme is bound to the substrates.

The Michaelis-Menten equation given by expression (11) was used here to calculate V_0, which is considered as the *RateConstant* parameter in expression (1).

$$V_0 = \frac{V_{MAX}[S]}{K_M + [S]} \quad (11)$$

The kinetic parameters of the different reactions were selected according to the values reported and cited in Tables 3 and 4. These values were used in the simulation phase, and they can be adjusted during the validation and calibration phase so that the simulation exhibits a behavior similar to the physiological one.

3) Validation/verification of the conceptual model. Review of the consistency of the model created.

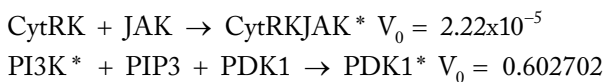*Simulation creation phase (based on the Big-Data Cellulat platform)*

4) Creation of the computational model (simulation). Registration of the cellular structures (cellular compartments) involved in the cell signaling system. This

Table 4. Examples of reactions and reactants defined during the formulation of the PI3K/Akt/mTOR signaling pathway model, including the xoconostle extract hypothesis.

REACTION	REACTANTS	INITIAL CONC. (μMOL)	K_M (μMOL)	V_{MAX} (μMOL/μL/S)	V_0
XOCOExt + Cyt + RK → XOCOExtCytRK	XOCOExt Cyt RK	0.028 0.1 0.25	34.2	7.6	2.22×10^{-5}
XOCOExtCytRK + JAK → XOCOExtCytRKJAK*	XOCOExt Cyt RK JAK	0.028 0.0001 0.25 0.11	34.2	7.6	2.22×10^{-5}
XOCOExtCytRKJAK* + STAT* → STAT	XOCOExt Cyt RK JAK STAT	0.028 0.0001 0.25 0.11 0.4	34.2 74.1	7.6 49	2.22×10^{-5} 0.263087248
STAT → INHIBITION PROLIFERATION	STAT	0.4	74.1	49	0.263087248
XOCOExtCytRKJAK* + SHP1* → XOCOExtCytRK + JAK	XOCOExt Cyt RK JAK SHP1	0.028 0.0001 0.25 0.11 0.045	34.2	7.6	2.22×10^{-5}
XOCOExt + GF + RTK → XOCOExtGFRTK	XOCOExt GF RTK	0.028 0.0001 0.25	34.2	7.6	2.22×10^{-5}

step refers to the creation of the simulation structures that will contain the reactions and reactants. That is, the cellular compartments such as membrane, cytosol, nucleus, etc. In computational simulation, each cell compartment is conceived as a space of tuples.

5) For each cell structure, record the chemical reactions that take place in it, together with their kinetic parameters. The reactions modeled in step 2), using expressions (4) to (10), are now registered as elements of the computational simulation using the same nomenclature in which they were formulated, as shown in the following examples:

$$CytRK + JAK \rightarrow CytRKJAK^* \; V_0 = 2.22 \text{x} 10^{-5}$$
$$PI3K^* + PIP3 + PDK1 \rightarrow PDK1^* \; V_0 = 0.602702$$

6) For each cell structure, record the reactants belonging to it, together with their initial molar concentration value. All the reactants involved in the reactions modeled in step 2) must be recorded together with their micromolar concentration as elements of the computational simulation, as shown in the following examples:

$$JAK \text{ Initial conc.} (\mu\text{mol}) = 0.012$$
$$PI3K \text{ Initial conc.} (\mu\text{mol}) = 0.9$$

Simulation execution phase (based on the Big–Data Cellulat platform)

7) Triggering the simulation run. Running the simulation means the iteration of steps 1 to 6 previously described in section 2.1.2.
8) Observation of the behavior of the simulated biological system, using the available graphical components (concentration/time curves, activity maps, dynamic table of concentration values over time, etc.).

Calibration and validation phase of the simulation (based on the Big–Data Cellulat platform)

9) Calibration. Adjust the parameters of the model of the simulated biological system, from the execution of a series of simulated scenarios, until an acceptable adjustment is achieved between the final cellular states produced by the simulation and those observed in the *in vitro* experiments and/or reported in the specialized literature.
10) Validation. Perform the analysis of differences between simulated and observed values, using statistical indices such as Mean Bias Error (MBE), Mean Absolute Error (MAE), Mean Square Error (MSE), and Root Mean Square Error (RMSE). See expressions (12) to (15) below.

11) Design the *in silico* experiments (hypotheses) that need to be corroborated on the basis of the executed simulation, describing, as the case may be, the new reactions and reactants to incorporate, concentration values and kinetic parameters to modify, key elements to observe, etc.

12) Record in the current simulation, as appropriate, the new reactions, reactants, concentration values and kinetic parameters, which model the *in silico* experiment.

13) Run the resulting new simulation and, if necessary, calibrate it.

14) Analysis and interpretation of the results of the *in silico* experiment.

Validation methodology

The validation of the simulation model was based on the analysis of differences between simulated values (*YEstimated)* and measured values (*YMeasured*), using statistical indices such as the Mean Bias Error (MBE), the Mean Absolute Error (MAE), the Mean Square Error (MSE), and the Root Mean Square Error (RMSE), given by expressions (12) to (15), respectively.

Mean Bias Error (*MBE)* is mainly used to calculate the average error in the simulation model, and it is given by expression (12).

$$MBE = \frac{1}{N} \sum_{i=1}^{N} \left(Y_i^{Estimated} - Y_i^{Measured} \right) \qquad (12)$$

Mean Absolute Error (MAE) is a measure of the difference between the measured values and the estimated values, and is given by expression (13).

$$MAE = \frac{1}{N} \sum_{i=1}^{N} \left| Y_i^{Measured} - Y_i^{Estimated} \right| \qquad (13)$$

Mean Squared Error (MSE) measures the average squared difference between the measured values and the estimated values, and it is given by expression (14).

$$MSE = \frac{1}{N} \sum_{i=1}^{N} \left(Y_i^{Measured} - Y_i^{Estimated} \right)^2 \qquad (14)$$

Root Mean Square Error (RMSE) is the square root of the MSE, and is given by expression (15).

$$RMSE = \sqrt{\frac{1}{N} \sum_{i=1}^{N} \left(Y_i^{Measured} - Y_i^{Estimated} \right)^2} \qquad (15)$$

where in equations (12)-(15):

- $Y_i^{Measured}$, $1 \leq i \leq N$, denotes the measured values.
- $Y_i^{Estimated}$, $1 \leq i \leq N$, denotes the estimated values.

In silico prediction

The *in silico* stage consisted of 2 main activities:

1. The modeling, simulation, verification and validation of the PI3K/AKT/mTOR signaling pathway in breast cancer cells was performed following the methodology described above. At this step, the cellular structures where the reactions take place, the reagents and the final cellular states involved in the signaling pathway were identified and characterized, which were subsequently verified and validated with parameters already known in the cancer cell.

2. The hypothesis approach was carried out to predict what happens when the extract is added to the cancerous cells, observing its behavior and establishing the probable action target points. The established hypothesis was the following: "the administration of xoconostle extract modulates the union of cytosines to its receptor, inhibiting the activation of transcription factors, STAT in particular, and giving as a result an inhibition in angiogenesis and cellular proliferation."

In vitro evaluation

Preparation and standardization of the extract. The crude aqueous extract was prepared from epicarp by maceration in a laminar flow hood. Once the epicarp was dried and powdered, 1.5 g was dissolved in 15 ml of distilled water. The mixture of powder and solvent was magnetically stirred at 45 °C for 10 minutes. Subsequently, the solution was removed from the heat and placed in a sterile tube appropriate to the volume of the mixture, which was vortexed for 10 minutes and then centrifuged at 4500 rpm in 2 10-minute cycles to recover the supernatant. The final product obtained was sterilized by filtration and stored in a sterile amber bottle, keeping it refrigerated for immediate use.

XTT cell proliferation assay. Cell proliferation was determined using the Roche XTT kit (Roche PN 11465015001) by seeding 5×10^4 cells in 96-well plates, adding increasing concentrations of xoconostle extract and determining the absorbance at 550 nm, using as a positive control doxorubicin hydrochloride, concentration 0.15 μg/μl for each cell type. The XTT method is a colorimetric assay to determine cell viability by quantifying the formazan generated by live cells from XTT (sodium 3′- [1- (phenylaminocarbonyl) -3,4-tetrazolium] -bis(4-methoxy-6-nitro) benzenesulfonic acid hydrate). The amount of formazan is directly proportional to the number of metabolically active cells in the culture.

1. Cell proliferation. Cells of different cell lines were cultured in T-75 boxes with appropriate culture medium supplemented with 10% fetal bovine serum and 1% antifungal antibiotic, MCF-7 (MEM, Sigma Aldrich) and MDA-MB-231 (DMEM, Sigma Aldrich), incubated at 37 °C in a humid atmosphere with 5% CO2.

2. Cell counting. When the cells reached 85% confluence, they were trypsinized with 1% Trypsin Solution to detach them from the box. They were observed under the microscope to ensure complete separation of the cells. To inhibit the action of trypsin, 8 ml of the corresponding culture medium was added and the cells were gently resuspended. The cell suspension was poured into a sterile 15 ml tube and centrifuged at 1500 rpm for 10 minutes. Once the sediment with the cells was obtained, the supernatant was removed and the cells were resuspended in 500 μl of supplemented medium. In a sterile 1.5 ml microcentrifuge tube, 45 μl of 1× PBS, 45 μl of 0.4% trypan blue solution and 10 μl of the cell suspension were added. We placed 10 μl of the obtained suspension for count in a Neubauer chamber. Once the result is obtained, the number of cells per ml of suspension is determined.

3. Proliferation assay. In a 96-well plate, 5000 cells per well were filtered and supplemented culture medium was added to a final volume of 200 μl per well and incubated for 24 hours. After incubation, cell characteristics were observed and the culture medium was removed, increasing volumes of xoconostle extract were added, in all cases leading to a final volume of 200 μl with supplemented medium. Incubation was carried out for 24 hours. After incubation time, 50 μl of XTT and 100 μl of supplemented medium were added, the culture was incubated for 4 hours and read on a microplate reader at 550 nm.

Flow cytometry. The analysis of the cell cycle phases was performed using the aqueous extract on MDA-MB- 231 and MCF-7 cell lines and taking as a control the untreated lines. The measurement was carried out using a FACScantoII flow cytometer, at a reading of 1000 events per second, using propidium iodide, excited at 493 and at an emission of 605 nm with a forward scatter detector FSC of 606 and a side scatter detector SSC of 493.

UV-Vis spectrophotometry. The spectrophotometric characterization of the aqueous extract of *Opuntia joconostle* was carried out using a NANODROP 1000. The absorbance of the extract is the result of the incident radiation partially absorbed by each of its components. This fact causes a transition between the energy levels of the substance, which depends on the amount of compound within the extract.

Results and discussion

The modeling of the PI3K/AKT/MTOR

Figure 3 shows the results of the initial phase of modeling, verification and validation of the PI3K/Akt/mTOR signaling pathway and the final cellular states involved. Subsequently, a second model of this signaling pathway was performed, including the reactions involving the xoconostle extract in the final cellular states. Tables 3 and 4 illustrate a small fragment of the reactions, reagents and kinetic parameters of the PI3K/Akt/mTOR signaling pathway and the reactions involving xoconostle extract, respectively, since the overall model involves more than 60 reactions and 70 reagents.
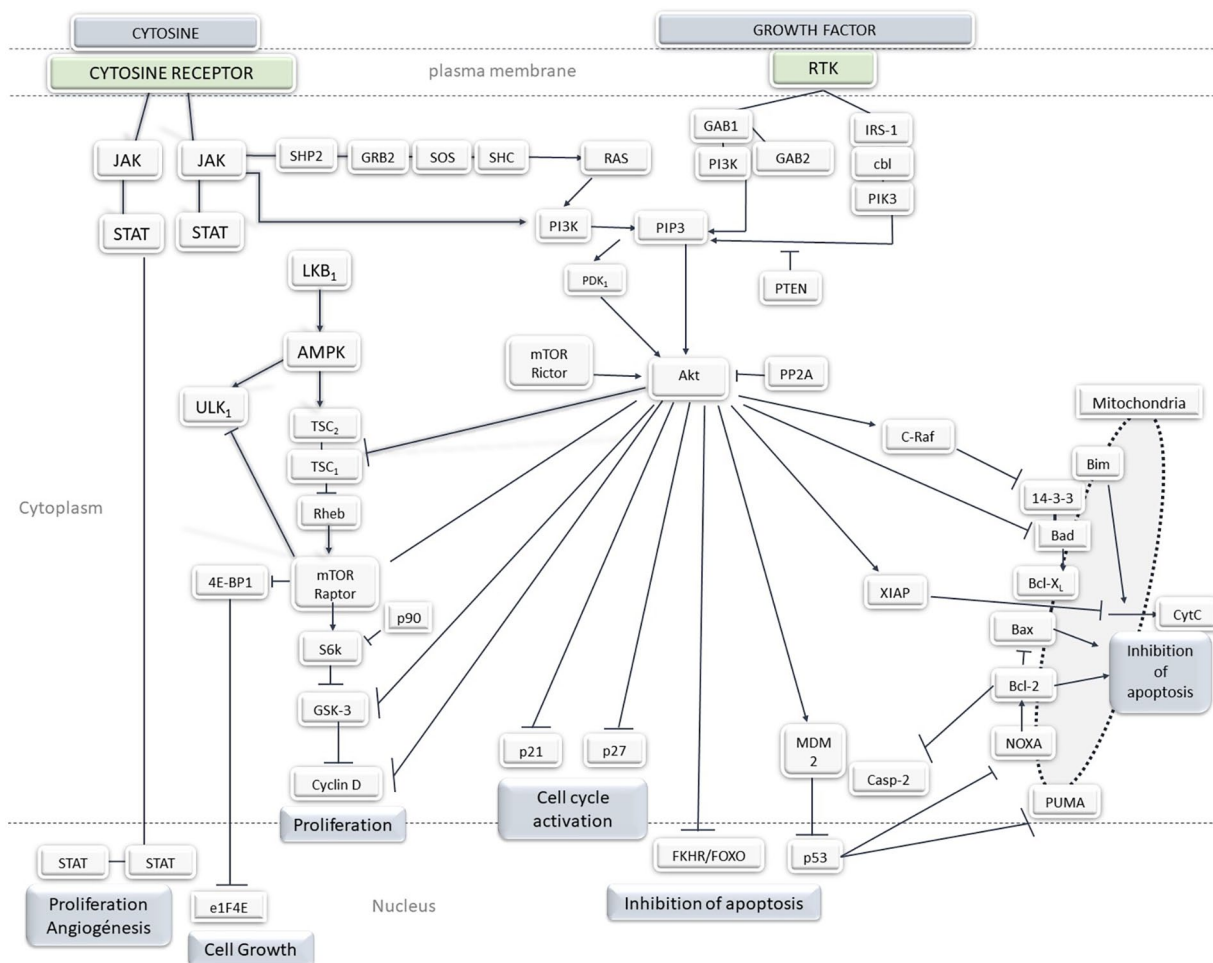
The simulation of the PI3K/AKT/mTOR

The *in silico* experimentation consisted in running the PI3K/Akt/mTOR simulation in the 2 scenarios previously considered in the model formulation: (a) the known PI3K/Akt/mTOR signaling pathway in cancer cells and (b) the same signaling pathway extended with the reactions and reagents that model the hypothesized role of xoconostle extract in inhibiting cell proliferation. As a part of the aforementioned methodology, the simulation creation phase is illustrated in Figures 4 and 5, where the translation of the previously formulated PI3K/Akt/mTOR model into simulation elements in the Cellulat bioinformatics platform can be seen. Figure 4 shows the creation of the reactions while Figure 5 illustrates the establishment of the reagents.

Through this first set of *in silico* experiments, in which the reactions that model the effect of the xoconostle extract on the final cellular states were not considered, it was possible to corroborate the following hypotheses about the expected behavior of this pathway in cancer cells (see Figure 6):

1. The binding of extracellular signaling molecules such as cytokines to their receptor results in the activation of JAK kinase, subsequently catalyzing series of tyrosine phosphorylation reactions that activate the transcription factor STAT for subsequent dimerization, whose activation is related to proliferation and angiogenesis.

2. The activation of PI3K and Akt leads to the sequential activation of the effector proteins mTOR, C-Raf, XIAP and MDMD which, after series of phosphorylations, lead to the inactivation of cyclin D, cyclin inhibitors such as p21 and p27, as well as transcription factors. The result is proliferation, angiogenesis, cell growth, cell cycle activation, and inhibition of apoptosis.

This first set of experiments confirmed that the binding of extracellular signaling molecules, such as cytosines, to the cytosine receptor results in the activation of JAK kinases, which are
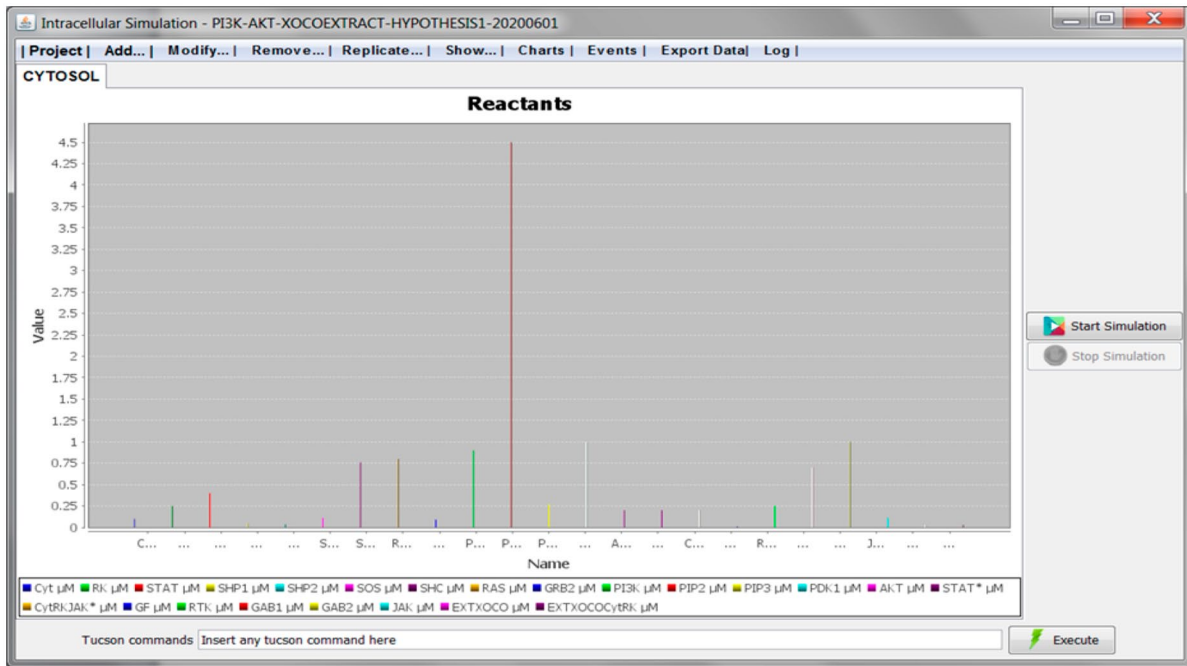
Figure 3. Model of the PI3k/Akt/mTOR signaling pathway. It shows the result of the modeling phase with the interactions and inhibitions of the components activated from cytosines, leading to proliferation and inhibition of apoptosis in a breast cancer cell.

Figure 4. Creation of the simulation of the PI3K/Akt/mTOR signaling pathway in the Big-Data Cellulat platform. Recording of chemical reactions.

bound to the receptor, to subsequently catalyze a series of tyrosine phosphorylation reactions that activate the transcription factor STAT. STAT activation led to phosphorylation of

the tyrosine residue and subsequent dimerization with another active STAT to form a homodimer, which is essential to facilitate passage from the cytoplasm to the nucleus and thus to

Figure 5. Creation of the simulation of the PI3K/Akt/mTOR signaling pathway in the Big-Data Cellulat platform. Recording and visualization of the reactants. signaling pathway simulation over time.

activate the gene transcription, resulting in proliferation and angiogenesis.

On the other hand, PI3K and Akt activation led to sequential activation of key effector proteins and cell proliferation. As a consequence of the activation of these effector proteins, the following cellular processes were triggered: 1) activation of XIAP and inactivation of Bcl-2 and Bcl-XL1 proteins, led to inhibition of apoptosis, 2) inhibition of cyclin D produced by Akt and inhibition of GSK-3 led to cell proliferation, 3) inhibition of p21 and p27 by Akt leading to cell cycle activation, 4) inhibition of FKHR/FOXO by Akt led to inhibition of apoptosis, and 5) activation of mTOR Raptor inhibiting 4E-BP1 and the latter in turn inhibiting e1f4E promoted cell growth. Simulation for the PI3K/Akt/mTOR pathway in the cancer cell corroborates that cytokine binding to the cytosine receptor triggers increased cell proliferation, angiogenesis and inhibition of apoptosis by different cascades involving STAT, Akt and BAX/Bcl-2 family members.[66-68]

Simulation validation

As mentioned earlier, the validation/verification of the PI3K/Akt/mTOR simulation was based on the analysis of differences between simulated values and measured values, using the statistical indices mean bias error (MBE), mean absolute error (MAE), mean squared error (MSE), and root mean square error (RMSE), previously introduced and given by expressions (4) to (7), respectively. The estimated and observed values refer to 8 key signaling elements located at the end of the different top-down signaling cascades that make up the PI3K/Akt/mTOR signaling pathway, whose activation/inhibition is

decisive in the triggering of some of the cellular processes that characterize this type of cancer cells (eg, proliferation, cell cycle activation and apoptosis inhibition). As can be seen in Figure 3, the target signaling elements are STAT, e1F4E, Cyclin D, p21, p27, FKHR/FOXO, XIAP, and Bcl-2.

Once the first simulation run was completed, the 4 types of errors were calculated. Observing that not all the expected final cellular states (see Figure 3) were reached, both the concentration values of signaling elements and the kinetic parameters of chemical reactions were modified, taking into account heuristics and the knowledge of the domain experts. Subsequently, the simulation was run again and the 4 types of errors were calculated again, which decreased significantly in relation to the first set of errors. However, the simulation was still not able to produce all the expected final cell states, so the process of guided modification of reactant concentration values and reaction kinetic parameters continued.

Finally, this simulation calibration process was stopped when the following 2 conditions were reached: 1) a non-significant variation was recorded between the set of errors calculated for one run and for the subsequent simulation run, and 2) the simulation was able to reproduce all the expected cell states. The initial, partial and final errors obtained for the calibrated simulation model are listed in Table 5.

Prediction of the antiproliferative effect of xoconostle extract on the PI3K/Akt/mTOR signaling pathway

The second stage of the *in silico* experiment was aimed to predict the antiproliferative effect of xoconostle extract by
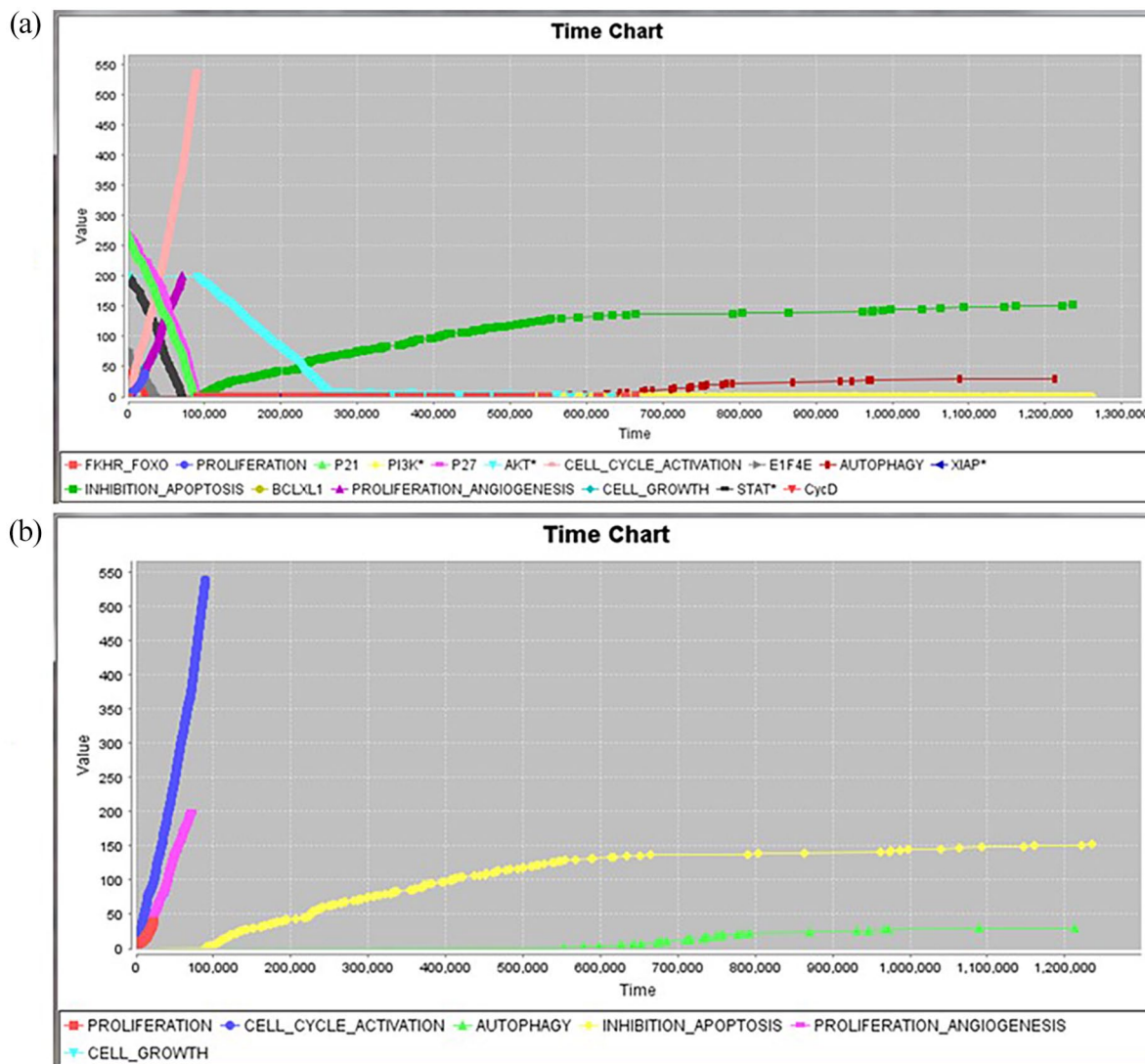
Figure 6. Simulation of the PI3K/Akt/mTOR signaling pathway over time: (a) simulation of the PI3K/Akt/mTOR pathway showing the different participants in each of the reactions that a cell undergoes to develop a cancerous process and (b) simulation in which the main actions necessary for the cell to start its cancerous process are observed, for example: the increase of apoptosis inhibition (in yellow) and the beginning of the presence of proliferation (red) and angiogenesis (pink).

modulating the PI3K/Akt/mTOR signaling pathway. Taking xoconostle extract concentrations as a starting point, increasing concentrations in multiples of 10 were tested. The results obtained in the *in silico* simulation before and after the application of *Opuntia joconostle* extract provided an overview of all the interactions between the different elements involved in the PI3K/Akt/mTOR signaling pathways, as well as a proposal of the likely therapeutic targets at a given LC_{50} for the extract, to be applied in the *in vitro* experimentation.

At this stage, where the simulation of the action of the extract on the cancer cell was carried out, the hypothesis previously stated was proved, in which it is established that the action of the xoconostle extract in the inhibition of cell proliferation is due to the binding of the components of the extract to the cytosine receptor, causing an antagonist effect,

preventing the union of cytosines to it; the mechanism prevents the activation of the transcription factor STAT and, consequently, it a decrease of the proliferation and angiogenesis process is observed, promoting cell apoptosis.

In the hypothesis explored (Figure 7), it was corroborated that once the xoconostle extract is added, it binds to the cytosine receptor and causes the phosphorylation of JAK, causing its activation in the first instance, but inhibiting the subsequent phosphorylation cascades. In this case specifically, we simulate the option of inhibiting STAT homodimerization and thus preventing its passage to the nucleus, resulting in an antiproliferative effect. This confirms, that the inactivation of STAT within this signaling pathway is a therapeutic option, being an ideal target point, since cancer cells are highly dependent on STAT activity.[62,69]

Table 5. Initial, partial, and final errors obtained during the validation process of the PI3K/Akt/mTOR simulation.

TARGET SIGNALING ELEMENT	EXPECTED CONCENTRATION VALUE (Mμ)	CONCENTRATION VALUE REACHED (Mμ)		
		FIRST RUN	KTH RUN	FINAL RUN
STAT*	0.4	0.0	0.1	0.2
e1F4E	0.078	0.0	0.033	0.076
Cyclin D	0.04	0.01	0.025	0.04
p21	0.27	0.1	0.17	0.24
p27	0.27	0.1	0.16	0.24
FKHR/FOXO	0.4	0.0	0.21	0.32
XIAP*	0.6	0.1	0.2	0.4
Bcl-2*	0.2	0.1	0.1	0.2
Statistical indices				
MBE	–	−0.231	−0.1575	−0.06775
MAE	–	0.231	0.1575	0.06775
MSE	–	0.645684	0.335225	0.0110255
RMSE	–	0.803544	0.578998	0.1050023
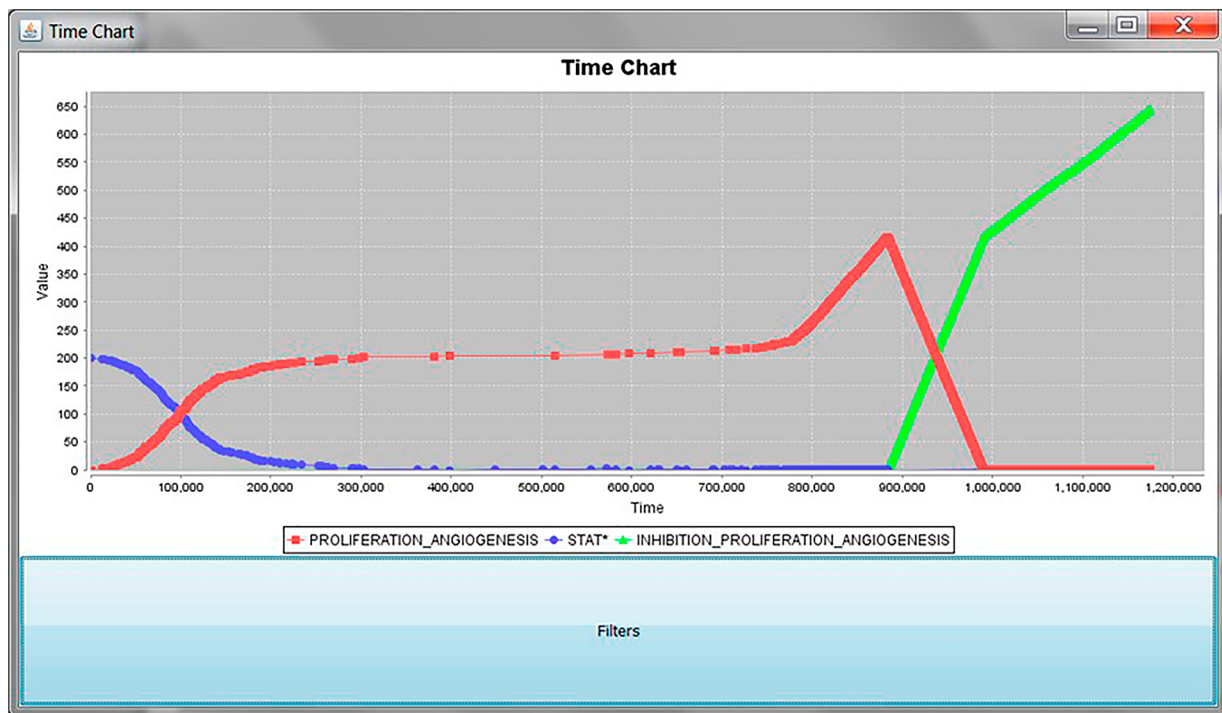
Figure 7. Behavior of the simulation of the PI3K/Akt/MTOR signaling pathway, considering the reactions that model the effect of the *O. joconostle* extract. At the *in silico* level, the hypothesis that the binding of the compounds to the cytokine receptor prevents STAT activation (blue curve) is corroborated. As a result, a decrease in cell proliferation (red curve) and an increase in the inhibition of angiogenesis (green curve) can be observed.

From the in silico prediction to the in vitro evaluation

After the *in silico* prediction phase, complementary *in vitro* experiments were carried out to corroborate the antiprolifera-tive action of the *O. joconostle* extract, using the concentrations of the extract proposed by the *in silico* experiments. The results obtained corroborated that the application of the aqueous extract at 24 hours on breast cancer cells led to an antiprolifera-tive effect on these cells, at lethal concentrations of 0.028 μg/μl for MCF-7 cells and 0.021 μg/μl for MDA-MB-231 cells
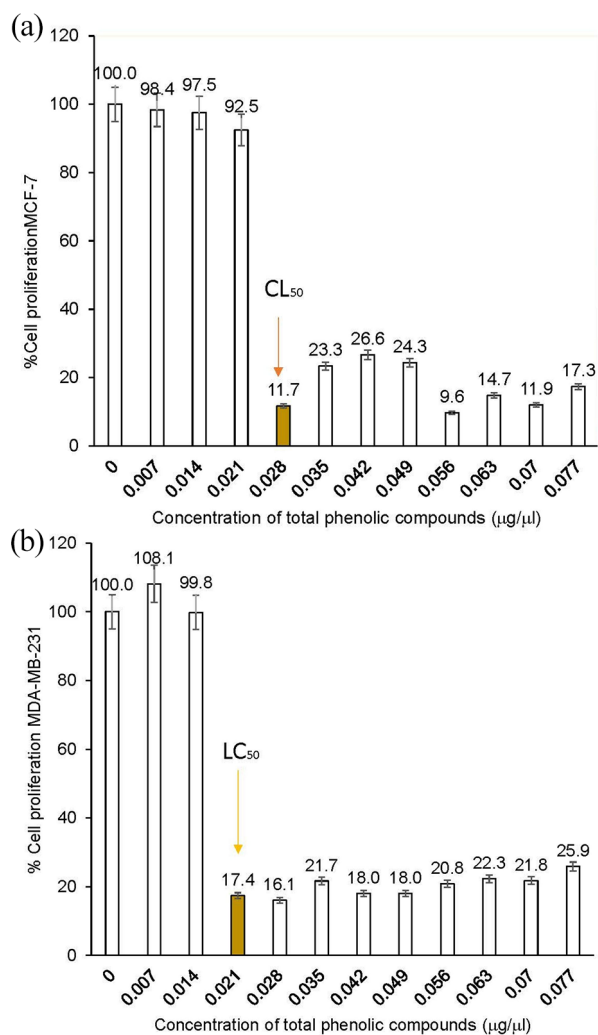
Figure 8. (a) Effect of conventional aqueous extract of *O. joconostle* on MCF-7, cell proliferation. The response of luminal breast cancer cell line A is shown for different concentrations of the extract with a proliferation of only 11.7% at a concentration of 0.028 µg/µl and (b) effect of the conventional aqueous extract of *O. joconostle* on MDA-MB-231, response in the triple negative cancer cell line with the extract at a concentration of 0.021 µg/µl presents a proliferation of 17.4%, less than 50%.

(Figure 8), making it clear that the antiproliferative activity of the extract depends on the dose used, similar to observations with other species of the genus Opuntia in different cell lines.[70]

Once the LC_{50} were detected, a flow cytometry was performed to know in which stage of the cycle the extract produced the arrest in the cell cycle progression. We obtained that the extract induces the arrest of cells in the G2/M phase, thus inhibiting cell proliferation and inducing apoptosis (see Figure 9). Moreover, the extract showed a similar action to that observed in the same breast cancer lines treated with the main flavonoids present in plant species, which arrest the cell cycle in the G2/M phase through mechanisms of action involving the participation of the PI3K/Akt/mTOR pathway.[71,72]

The UV-Vis spectrophotometric analysis of the aqueous extract of Opunta joconostle, allowed us to identify in a general way the functional groups present in the extract, thus visualizing the presence of phenolic compounds and flavonoids, groups located within the absorbance range of 220 to 375 nm.[73,74]

The absorbance obtained in the UV-vis spectrum coincided with that reported by Abou-Elella and Mohamed-Ali77, in 2014, where they relate the number of phenolic compounds of species of the Opuntia genus, with an antitumor effect on cancer cells. Phenolic compounds, or their mixture, synergistically confer antiproliferative activity on breast cancer cells. To continue this work, the extract will be analyzed by HPLC and NMR to identify the compounds present in the extract and those responsible for the antiproliferative activity.

Conclusions

The multidisciplinary work in the research of new drugs against cancer together with the use of computational simulation and *in silico* prediction models, such as the scenario provided by the Big- Data Cellulat bioinformatics platform, allows to reduce costs and time in the laboratory experimentation phases *in vitro* and *in vivo*, to determine the effect of new treatments against breast cancer.[75]

Through the use of the Big Data Cellulat platform, the researcher has a more detailed understanding of each of the reactions involved in the PI3K/Akt/mTOR pathway in a cancer cell and can put forward various hypotheses that propose the action of a substance as a treatment on it. For the PI3K/Akt/mTOR signaling pathway, cell proliferation, angiogenesis and inhibition of apoptosis are given mainly by the activation of JAK, STAT by the binding of extracellular signaling molecules such as cytokines to their receptor and also by the activation of PI3K and Akt leading to the activation of effector proteins such as mTOR, C-Raf, XIAP, and MDMD, which inactivate p21 and p27, and different transcription factors. The hypothesis formulated theoretically was accurate in the prediction thus supporting that the administration of *O. joconostle* extract modulates the binding of cytosines to its receptor, thus preventing the activation of JAK and the dimerization of the transcription factor STAT, resulting in the inhibition of angiogenesis and a decrease in cell proliferation.

The ability to implement *in silico* models prior to *in vitro* experimentation in the laboratory, allows to predict the effect of the substances under study, whether drugs or natural products, such as the extract of *O. joconostle*, by analyzing the possible effects of the extract showing a range of concentrations from which the extract of *O. joconostle* can present the effect *in vitro*.

Finally, it is predicted *in silico* and tested *in vitro* that *O. joconostle* extract has an antiproliferative effect on breast cancer cell lines at 0.028 µg/µl in MCF-7 (luminal A) cells and 0.021 µg/µl in MDA-MB-231 (triple negative) cells, these doses are higher than those reported with doxorubicin[76] treatment which is a drug currently employed at the clinical level.[77] The extract is also considered to play a very important role in
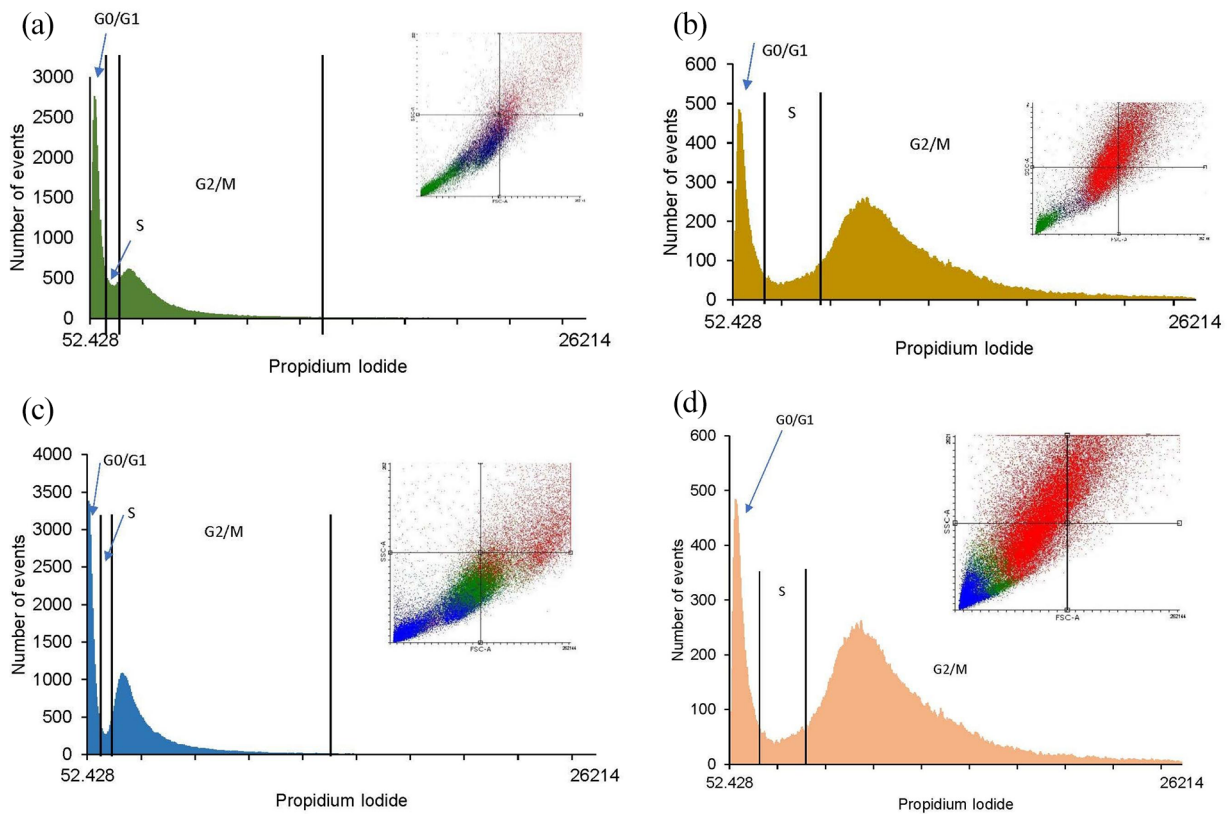
Figure 9. (a) The histogram of MCF-7 cells shows the distribution of the cell cycle phases of the control sample with a higher distribution of cells in the G0/G1 phase, (b) flow histogram of MCF-7 cells, 24 hours after treatment with the extract of *Opuntia joconostle* at a concentration of phenolic compounds of 0.035 μg/μl, which shows a higher distribution of cells in the G2/M phase, (c) histogram of MDA.MB.231 cells, shows the distribution of the cell cycle phases of the control sample, finding a higher percentage of cells distributed in the Go/G1 phase, and (d) histogram of cells MDA.MB.231, showing the distribution of the cell cycle phases 24 hours after the treatment with the aqueous extract of *Opuntia joconostle* at a concentration of phenolic compounds of 0.021 μg/μl): it distributes the population mainly to the G2/M phase.

cell cycle regulation by causing cell arrest, in both cell lines, in the G2/M phase, thus preventing the cells from achieving cell division, resulting in decreased proliferation.

From the conclusions and results obtained in this work, it is considered that in the future some of the components of *O. joconostle* extract could have a key role in the treatment of breast cancer, acting on the regulation of the PI3K/Akt/mTOR signaling pathway.

Acknowledgements

Author contributions

Conceived the PI3K/AKT/mTOR signaling model, including reactants, reactions, initial concentrations and kinetic parameters; developed the *in silico* and *in vitro* experiments, and wrote the first draft of the article: AO-G. Coordinated the use of the computational simulation and the in *silico* study, coordinated the modeling and simulation of PI3K/AKT/mTOR signaling network, jointly developed the structure and arguments for the article, and wrote the first draft of the article: PPG-P. Conceived the main ideas of the research project, validated and verified the PI3K/AKT/mTOR signaling model, including reactants, reactions and kinetic parameters, coordinated the in *silico* and in *vitro* experiments, and wrote the first draft of the article: MC-G. Coordinated the supply, preparation and standardization of the O. Joconostle extract and the design of in vitro evaluation. Contributed to the writing and review of the article: MGH-L. All authors reviewed and approved the final article.

ORCID iDs

Pedro Pablo González-Pérez https://orcid.org/0000-0001-7223-9035

Maura Cárdenas-García https://orcid.org/0000-0002-6114-1670

María Guadalupe Hernández-Linares https://orcid.org/0000-0001-9413-4322

REFERENCES

1. Global Cancer Observatory Mexico. Mexico. World Health Organization. 2020. https://gco.iarc.fr/today/data/factsheets/populations/484-mexico-fact-sheets.pdf (accessed 2020).
2. Reynoso NN, Torres-Dominguez JA. Epidemiología del cáncer en México: carga global y proyecciones 2000-2020. *Lat Am J Behav Med*. 2017;8(1). http://www.revistas.unam.mx/index.php/rlmc/article/view/65111

3.   Khan KH, Yap TA, Yan L, Cunningham D. Targeting the PI3K-AKT-mTOR signaling network in cancer. *Chin J Cancer*. 2013;32:253-265.

4.   Yan Y, Serra V, Prudkin L, et al. Evaluation and clinical analyses of downstream targets of the Akt inhibitor GDC-0068. *Clin Cancer Res*. 2013;19:6976-6986.

5.   Feng Y, Spezia M, Huang S, et al. Breast cancer development and progression: risk factors, cancer stem cells, signaling pathways, genomics, and molecular pathogenesis. *Genes Dis*. 2018;5:77-106.

6.   Guerrero-Zotano A, Mayer IA, Arteaga CL. PI3K/AKT/mTOR: role in breast cancer progression, drug resistance, and treatment. *Cancer Metastasis Rev*. 2016;35:515-524.

7.   Mukohara T. PI3K mutations in breast cancer: prognostic and therapeutic implications. *Breast Cancer Target Ther*. 2015;7:111-123.

8.   Paplomata E, O'Regan R. The PI3K/AKT/mTOR pathway in breast cancer: targets, trials and biomarkers. *Ther Adv Med Oncol*. 2014;6(4):154-166. doi:10.1177/1758834014530023

9.   Yu WK, Xu ZY, Yuan L, et al. Targeting β-catenin signaling by natural products for cancer prevention and therapy. *Front Pharmacol*. 2020;11:984.

10. Zhang X, Tang N, Hadden TJ, Rishi AK. Akt, FoxO and regulation of apoptosis. *Biochim Biophys Acta - Mol Cell Res*. 2011;1813:1978-1986.

11. Chalhoub N, Baker SJ. PTEN and the PI3-kinase pathway in cancer. *Annu Rev Pathol Mech Dis*. 2009;4:127-150.

12. Abell K, Watson CJ. The Jak/Stat pathway: a novel way to regulate PI3K activity. *Cell Cycle*. 2005;4:897-900.

13. Vogt PK, Hart JR. PI3K and STAT3: a new alliance. *Cancer Discov*. 2011;1:481-486.

14. Cai X. Exact stochastic simulation of coupled chemical reactions with delays. *J Chem Phys*. 2007;126:124108.

15. Engblom S. Stochastic simulation of pattern formation in growing tissue: a multilevel approach. *Bull Math Biol*. 2019;81:3010-3023.

16. Ramsey S, Orrell D, Bolouri H. Dizzy: stochastic simulation of large-scale genetic regulatory networks. *J Bioinform Comput Biol*. 2011;3:415-436.

17. Konrad L, Scheiber JA, Völck-Badouin E, et al. Alternative splicing of TGF-betas and their high-affinity receptors TβRI, TβRII and TβRIII (betaglycan) reveal new variants in human prostatic cells. *BMC Genomics*. 2007;8:318.

18. Hoops S, Sahle S, Gauges R, et al. COPASI--a COmplex PAthway SImulator. *Bioinformatics*. 2006;22:3067-3074.

19. Kent E, Hoops S, Mendes P. Condor-COPASI: high-throughput computing for biochemical networks. *BMC Syst Biol*. 2012;6:1-13.

20. Hepburn I, Chen W, Wils S, De Schutter E. STEPS: efficient simulation of stochastic reaction-diffusion models in realistic morphologies. *BMC Syst Biol*. 2012;6:36.

21. Cardelli L, Perez-Verona IC, Tribastone M, Tschaikowski M, Vandin A, Waizmann T. Exact maximal reduction of stochastic reaction networks by species lumping. *Bioinformatics*. 2021;37:2175-2182.

22. Naldi A, Hernandez C, Levy N, et al. The CoLoMoTo interactive notebook: accessible and reproducible computational analyses for qualitative biological networks. *Front Physiol*. 2018;9:680.

23. Balazki P, Lindauer K, Einloft J, Ackermann J, Koch I. MONALISA for stochastic simulations of Petri net models of biochemical systems. *BMC Bioinformatics*. 2015;16:1-11.

24. Kuwahara H, Mura I. An efficient and exact stochastic simulation method to analyze rare events in biochemical systems. *J Chem Phys*. 2008;129:165101.

25. Voliotis M, Thomas P, Grima R, Bowsher CG. Stochastic simulation of biomolecular networks in dynamic environments. *PLoS Comput Biol*. 2016;12:e1004923.

26. Ghosh D, De RK. Block Search Stochastic Simulation Algorithm (BlSSSA): a fast stochastic simulation algorithm for modeling large biochemical networks. *IEEE/ACM Trans Comput Biol Bioinform*. 2021;99:1-1. doi:10.1109/TCBB.2021.3070123

27. Petrov T. Markov chain aggregation and its application to rule-based modelling. *Methods Mol Biol*. 2019;1945:297-313.

28. Ge H, Qian M. Boolean network approach to negative feedback loops of the p53 pathways: synchronized dynamics and stochastic limit cycles. *J Comput Biol*. 2009;16:119-132.

29. Chiam KH, Tan CM, Bhargava V, Rajagopal G. Hybrid simulations of stochastic reaction-diffusion processes for modeling intracellular signaling pathways. *Phys Rev E Stat Nonlin Soft Matter Phys*. 2006;74:051910.

30. Welf ES, Haugh JM. Stochastic models of cell protrusion arising from spatiotemporal signaling and adhesion dynamics. *Methods Cell Biol*. 2012;110:223-241.

31. Sanchez-Vega F, Mina M, Armenia J, et al. Abstract 3302: the molecular landscape of oncogenic signaling pathways in The Cancer Genome *Atlas. Cell*. 2018;173:321-337.e10.

32. Bouhaddou M, Barrette AM, Stern AD, et al. A mechanistic pan-cancer pathway model informed by multi-omics data interprets stochastic cell fate responses to drugs and mitogens. *PLoS Comput Biol*. 2018;14:e1005985.

33. Ganesan N, Li J, Sharma V, Jiang H, Compagnoni A. Process simulation of complex biological pathways in physical reactive space and reformulated for massively parallel computing platforms. *IEEE/ACM Trans Comput Biol Bioinform*. 2016;13:365-379.

34. Sehl ME, Shimada M, Landeros A, Lange K, Wicha MS. Modeling of cancer stem cell state transitions predicts therapeutic response. *PLoS One*. 2015;10:e0135797.

35. Sabbe N, Thas O, Ottoy JP. EMLasso: logistic lasso with missing data. *Stat Med*. 2013;32:3143-3157.

36. Liu Y, Purvis J, Shih A, Weinstein J, Agrawal N, Radhakrishnan R. A multiscale computational approach to dissect early events in the Erb family receptor mediated activation, differential signaling, and relevance to oncogenic transformations. *Ann Biomed Eng*. 2007;35:1012-1025.

37. Calabrese EJ, Priest ND, Kozumbo WJ. Thresholds for carcinogens. *Chem Biol Interact*. 2021;341:109464.

38. Khatibi S, Zhu HJ, Wagner J, Tan CW, Manton JH, Burgess AW. Mathematical model of TGF-βsignalling: feedback coupling is consistent with signal switching. *BMC Syst Biol*. 2017;11:48.

39. Zielinski R, Przytycki PF, Zheng J, Zhang D, Przytycka TM, Capala J. The crosstalk between EGF, IGF, and insulin cell signaling pathways—computational and experimental analysis. *BMC Syst Biol*. 2009;3:88.

40. Haack F, Lemcke H, Ewald R, Rharass T, Uhrmacher AM. Spatio-temporal model of endogenous ROS and raft-dependent WNT/beta-catenin signaling driving cell fate commitment in human neural progenitor cells. *PLoS Comput Biol*. 2015;11:e1004106.

41. Kogan Y, Halevi-Tobias KE, Hochman G, Baczmanska AK, Leyns L, Agur Z. A new validated mathematical model of the Wnt signalling pathway predicts effective combinational therapy by sFRP and Dkk. *Biochem J*. 2012;444:115-125.

42. Vargas DA, Sun M, Sadykov K, Kukuruzinska MA, Zaman MH. The integrated role of Wnt/β-catenin, N-glycosylation, and E-cadherin-mediated adhesion in network dynamics. *PLoS Comput Biol*. 2016;12:e1005007.

43. Agur Z, Kirnasovsky OU, Vasserman G, et al. Dickkopf1 regulates fate decision and drives breast cancer stem cells to differentiation: an experimentally supported mathematical model. *PLoS One*. 2011;6:e24225.

44. Gérard C, Di-Luoffo M, Gonay L, et al. Dynamics and predicted drug response of a gene network linking dedifferentiation with beta-catenin dysfunction in hepatocellular carcinoma. *J Hepatol*. 2019;71:323-332.

45. Kay SK, Harrington HA, Shepherd S, et al. The role of the Hes1 crosstalk hub in Notch-Wnt interactions of the intestinal crypt. *PLoS Comput Biol*. 2017;13:e1005400.

46. Gou J, Lin L, Othmer HG. A model for the Hippo pathway in the Drosophila wing disc. *Biophys J*. 2018;115:737-747.

47. Gupta S, Silveira DA, Mombach JCM. Towards DNA-damage induced autophagy: a Boolean model of p53-induced cell fate mechanisms. *DNA Repair*. 2020;96:102971.

48. Gong H, Zuliani P, Komuravelli A, Faeder JR, Clarke EM. Analysis and verification of the HMGB1 signaling pathway. *BMC Bioinformatics*. 2010;11 Suppl 7:S10.

49. Elizalde S, Laughney AM, Bakhoum SF. A Markov chain for numerical chromosomal instability in clonally expanding populations. *PLoS Comput Biol*. 2018;14:e1006447.

50. Ciocchetta F, Duguid A, Guerriero ML. A compartmental model of the cAMP/PKA/MAPK pathway in Bio-PEPA. *Electron Proc Theor Comput Sci EPTCS*. 2009;11:71-90.

51. Kerr RA, Bartol TM, Kaminsky B, et al. Fast Monte Carlo simulation methods for biological reaction-diffusion systems in solution and on surfaces. *SIAM J Sci Comput*. 2008;30:3126.

52. Cowan AE, Moraru II, Schaff JC, Slepchenko BM, Loew LM. Spatial modeling of cell signaling networks. *Methods Cell Biol*. 2012;110:195-221.

53. Swat MH, Thomas GL, Belmonte JM, Shirinifard A, Hmeljak D, Glazier JA. Multi-scale modeling of tissues using CompuCell3D. *Methods Cell Biol*. 2012;110:325-366.

54. Cárdenas-García M, González-Pérez PP, Montagna S, Cortés OS, Caballero EH. Modeling intercellular communication as a survival strategy of cancer cells: an in silico approach on a flexible bioinformatics framework. *Bioinform Biol Insights*. 2016;10:5-18.

55. González-Pérez PP, Cárdenas-García M. Inspecting the role of PI3K/AKT signaling pathway in cancer development using an in silico modeling and simulation approach. In: Lecture Notes in Computer Science (Including Subseries Lecture Notes in Artificial Intelligence and Lecture Notes in Bioinformatics). Vol 10813 LNBI. Springer Verlag; 2018:83-95. doi:10.1007/978-3-319-78723-7_7

56. Cárdenas-García M, González-Pérez PP. An in silico approach for understanding the complex intercellular interaction patterns in cancer cells. In: BIOINFORMATICS 2018 - 9th International Conference on Bioinformatics Models, Methods and Algorithms, *Proceedings; Part of 11th International Joint Conference on Biomedical Engineering Systems and Technologies, BIOSTEC 2018. Vol 3. SciTePress; 2018*:188-195. doi:10.5220/0006722601880195

57. González PP, Cárdenas M, Camacho D, Franyuti A, Rosas O, Lagúnez-Otero J. Cellulat: an agent-based intracellular signalling model. *Bio Syst*. 2003;68:171-185.

58. Gelernter D. Generative communication in Linda. *ACM Trans Program Lang Syst*. 1985;7:80-112.
59. González-Pérez PP, Cárdenas-García M. Modeling and simulation of molecular mechanism of action of dietary polyphenols on the inhibition of anti-apoptotic PI3K/AKT pathway. *Comput Mol Biosci*. 2013;03:39-52.
60. Rossi D, Cabri G, Denti E. Tuple-based technologies for coordination. *Coord Internet Agents*. Published online 2001;1:83-109. doi:10.1007/978-3-662-04401-8_4
61. Cokic VP, Bhattacharya B, Beleslin-Cokic BB, Noguchi CT, Puri RK, Schechter AN. JAK-STAT and AKT pathway-coupled genes in erythroid progenitor cells through ontogeny. *J Transl Med*. 2012;10:116.
62. Furqan M, Akinleye A, Mukhi N, Mittal V, Chen Y, Liu D. STAT inhibitors for cancer therapy. *J Hematol Oncol*. 2013;6:90.
63. Mizuguchi R, Noto S, Yamada M, Ashizawa S, Higashi H, Hatakeyama M. Ras and signal transducer and activator of transcription (STAT) are essential and sufficient downstream components of Janus kinases in cell proliferation. *Japanese J Cancer Res*. 2000;91:527-533.
64. Hofler A, Nichols T, Grant S, et al. Study of the PDK1/akt signaling pathway using selective PDK1 inhibitors, HCS, and enhanced biochemical assays. *Anal Biochem*. 2011;414:179-186.
65. Zhang H, Hannon GJ, Beach D. p21-containing cyclin kinases exist in both active and inactive states. *Genes Dev*. 1994;8:1750-1758.
66. Lim CP, Cao X. Structure, function, and regulation of STAT proteins. *Mol Biosyst*. 2006;2:536-550.
67. Nicholson KM, Anderson NG. The protein kinase B/Akt signalling pathway in human malignancy. *Cell Signal*. 2002;14:381-395.
68. Brady HJM, Gil-Gómez G. Molecules in focus bax. The pro-apoptotic Bcl-2 family member, bax. *Int J Biochem Cell Biol*. 1998;30:647-650.
69. Frank DA. STAT signaling in the pathogenesis and treatment of cancer. *Mol Med*. 1999;5(7):432-456. doi:10.1007/BF03403538
70. Kim J, Soh SY, Shin J, Cho CW, Choi YH, Nam SY. Bioactives in cactus (Opuntia ficus-indica) stems possess potent antioxidant and pro-apoptotic activities through COX-2 involvement. *J Sci Food Agric*. 2015;95:2601-2606.
71. Zhu L, Xue L. Kaempferol suppresses proliferation and induces cell cycle arrest, apoptosis, and DNA damage in breast cancer cells. *Oncol Res*. 2019;27:629-634.
72. Cao L, Yang Y, Ye Z, et al. Quercetin-3-methyl ether suppresses human breast cancer stem cell formation by inhibiting the Notch1 and PI3K/Akt signaling pathways.. *Int J Mol Med*. 2018;42:1625-1636.
73. Martínez-Valverde I, Periago MJ, Ros G. Significado nutricional de los compuestos fenólicos de la dieta. *Arch Latinoam Nutr*. 2000;50:5-18.
74. Hess S, Alvarez JL, Iturra G, Romero M. Evidence of UVB differential response in Sophora microphylla from shady and sunny places. *J Chil Chem Soc*. 2002;47:501-510.
75. M. Abou Elella F. Antioxidant and anticancer activities of different constituents extracted from Egyptian prickly pear cactus (Opuntia ficus-indica) peel. *Biochem Anal Biochem*. 2014;3(4):1-9. doi:10.4172/2161-1009.1000158
76. Abu N, Akhtar MN, Ho WY, Yeap SK, Alitheen NB. 3-bromo-1-hydroxy-9,10-anthraquinone (BHAQ) inhibits growth and migration of the human breast cancer cell lines MCF-7 and MDA-MB231. *Molecules*. 2013;18:10367-10377.
77. Wen SH, Su SC, Liou BH, Lin CH, Lee KR. Sulbactam-enhanced cytotoxicity of doxorubicin in breast cancer cells. *Cancer Cell Int*. 2018;18:128.